Notch signaling regulates murine atrioventricular conduction and the formation of accessory pathways

Stacey Rentschler,[1,2] Brett S. Harris,[3] Laura Kuznekoff,[4] Rajan Jain,[1,2] Lauren Manderfield,[1] Min Min Lu,[2] Gregory E. Morley,[4] Vickas V. Patel,[2] and Jonathan A. Epstein[1,2]

[1]Department of Cell and Developmental Biology and Institute for Regenerative Medicine, and [2]Penn Cardiovascular Institute, University of Pennsylvania, Philadelphia, Pennsylvania, USA. [3]Medical University of South Carolina, Charleston, South Carolina, USA. [4]New York University, New York, New York, USA.

Ventricular preexcitation, which characterizes Wolff-Parkinson-White syndrome, is caused by the presence of accessory pathways that can rapidly conduct electrical impulses from atria to ventricles, without the intrinsic delay characteristic of the atrioventricular (AV) node. Preexcitation is associated with an increased risk of tachyarrhythmia, palpitations, syncope, and sudden death. Although the pathology and electrophysiology of preexcitation syndromes are well characterized, the developmental mechanisms are poorly understood, and few animal models that faithfully recapitulate the human disorder have been described. Here we show that activation of Notch signaling in the developing myocardium of mice can produce fully penetrant accessory pathways and ventricular preexcitation. Conversely, inhibition of Notch signaling in the developing myocardium resulted in a hypoplastic AV node, with specific loss of slow-conducting cells expressing connexin-30.2 (Cx30.2) and a resulting loss of physiologic AV conduction delay. Taken together, our results suggest that Notch regulates the functional maturation of AV canal embryonic myocardium during the development of the specialized conduction system. Our results also show that ventricular preexcitation can arise from inappropriate patterning of the AV canal–derived myocardium.

Introduction

In the embryonic heart, the atrial myocardium is separated from ventricular myocardium by a circumferential band of atrioventricular (AV) canal cardiomyocytes that conduct electrical impulses slowly, resulting in AV delay, which facilitates unidirectional blood flow (1, 2). Embryonic AV canal cells ultimately give rise to myocardium within the lower rim of the atria, myocardium supporting the AV valves, specialized conducting cells of the AV node, and a portion of the left ventricular free wall (3). During early gestation and midgestation in the mouse, AV canal myocytes have an immature contractile network and express low conductance gap junctions, thereby conferring slow conduction. They proliferate more slowly than atrial and ventricular myocytes and can be distinguished from adjacent atrial and ventricular myocytes by expression of genes, including *Tbx2/3*, and bone morphogenetic protein 2 (*Bmp2*), and by a relative absence of Notch signaling (2, 4–6). During late gestation, a significant number of AV canal myocytes undergo apoptosis (7). At the same time, epicardial cells in the region of the AV junction undergo epithelial-to-mesenchymal transformation and invade the heart to form the annulus fibrosis, an insulating plane of nonconductive tissue separating the atria and ventricles (8, 9). As a result of these coordinated events, embryonic AV electrical continuity is lost, and conduction from atria to ventricles is funneled through the specialized conduction system of the AV node and His-Purkinje system (10).

The mature AV node is composed of numerous cell types, including a population of myocytes derived from AV canal myocardium (3). The AV node performs a similar function to that of the embryonic AV canal, in that it delays electrical impulses originating in the atria before they are allowed to excite the ventricles, thereby allowing coordinated contraction of the atria prior to ventricular systole and facilitating forward blood flow. The developmental processes regulating formation of the AV node from embryonic AV canal cardiomyocytes are just beginning to be elucidated. Bmp and Notch signaling pathways have been implicated in boundary formation between AV canal and atrium/ventricle and perhaps in maturation of AV canal derivatives (2). In the zebrafish heart, for example, knockdown of *notch1b* results in a failure to develop physiologic AV delay and a prolonged refractory period within the AV canal (11). Expression of activated Notch during early heart formation disrupts AV canal myocardium boundaries and leads to midgestation lethality (12). T-box genes, including *Tbx2*, *Tbx3*, and *Tbx5*, Nkx2.5, and Gata factors have also been implicated (reviewed in ref. 2). For example, $Tbx5^{+/-}$ mice have reduced expression of *Tbx3* and the low conductance gap junction connexin-30.2 (*Cx30.2*) in the AV canal (13, 14).

Ventricular preexcitation occurs when an electrically active muscular connection, apart from the AV node-His pathway, exists between the atrium and ventricle and can lead to symptomatic tachycardia or sudden death as the first clinical manifestation. Wolff-Parkinson-White syndrome (WPW) is most commonly diagnosed in children or young adults, with a prevalence of approximately 0.2% (15–17). It is the second most common cause of reentrant supraventricular tachycardia in the Western world and the most common cause in China (18). The presence of dual AV electrical connections (the AV node and the accessory pathway) with different conduction velocities and refractory periods provides the substrate for initiation and perpetuation of reentrant tachycardia. In addition, for reasons that are not well understood, atrial fibrillation develops in up to one-third of WPW patients at a young age. The occurrence of atrial fibrillation in the presence of an accessory pathway that conducts rapidly can be life threatening, because the rapid ventricular response may lead to ventricular fibrillation.

Conflict of interest: The authors have declared that no conflict of interest exists.
Citation for this article: *J Clin Invest.* 2011;121(2):525–533. doi:10.1172/JCI44470.

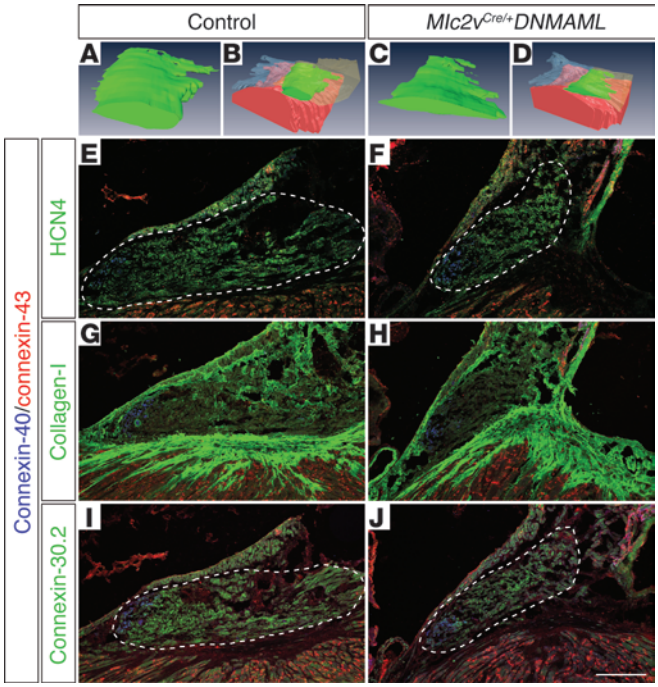

Figure 1
Loss of Notch signaling results in a smaller AV node and alteration of connexin-expressing cells. 3D reconstruction from trichrome-stained images of the AV node of a representative control heart is shown in **A** and **B** (different renderings of the same reconstruction; AV node volume = 8.2×10^6 μm^3 in this heart) and the AV node of a *Mlc2v*$^{Cre/+}$*DNMAML* mutant is shown in **C** and **D** (different renderings of the same reconstruction; AV node volume = 3.5×10^6 μm^3). (**A**–**D**) AV nodal tissue is green, ventricular myocardium is red, tricuspid valve is transparent blue, and (**B** and **D**) atrial septum is transparent yellow. (**E** and **F**) Immunohistochemistry demonstrates a reduction of HCN4-positive AV nodal cells in *Mlc2v*$^{Cre/+}$*DNMAML* mutants compared with that of control littermates. (**G** and **H**) Collagen I staining reveals an intact annulus fibrosis in *Mlc2v*$^{Cre/+}$*DNMAML* mutants when compared with control. (**I** and **J**) There is a selective loss of connexin-30.2–positive AV nodal cells in *Mlc2v*$^{Cre/+}$*DNMAML* mutants, with a maintenance of connexin-40–positive lower nodal cells. (**E**–**J**) Connexin-43 is not ectopically upregulated in *Mlc2v*$^{Cre/+}$*DNMAML* mutants. Control animals are littermate *Mlc2v*$^{+/+}$*DNMAML* animals. Dashed lines delineate the compact AV node in **E**, **F**, **I**, and **J**. Scale bar: 100 μm (**E**–**J**).

WPW is most commonly a sporadic and isolated cardiac disorder, although autosomal dominant familial inheritance has been described (19) as has association with congenital heart disease, especially Ebstein's anomaly (20). There are 2 known genetic associations with WPW in humans. Mutations in the AMP-activated protein kinase γ-2 subunit (PRKAG2) result in a rare form of WPW in the setting of a glycogen storage cardiomyopathy (21–23). Microdeletions of *BMP2* have recently been associated with a syndrome of WPW with either cognitive dysfunction or Alagille syndrome (24, 25). In mice, deletion of a BMP receptor within the embryonic AV canal leads to a low penetrance of both accessory pathways and AV nodal defects (26, 27). Of interest, the gene encoding a Notch ligand, *JAGGED1*, known to be associated with Alagille syndrome (28, 29), is located 3.8-MB centromeric to *BMP2* and is also deleted in some of these patients. This raises the question of whether altered Notch signaling may contribute to the observed preexcitation in this syndrome.

Here we provide evidence that Notch signaling can modulate late stages of AV canal myocardial maturation. Our data indicate that inhibition of Notch signaling can impede normal development of the AV node and can lead to a selective loss of slow-conducting cells, characteristic of the mature AV node. Conversely, activation of Notch signaling in the mouse induces ventricular preexcitation. Notch-activated mice survive gestation and develop electrophysiologic evidence of ventricular preexcitation only after birth. We propose that WPW and other AV conduction disorders may result from aberrations in Notch signaling and abnormal persistence or regression of AV canal myocardial derivatives.

Results

Notch inhibition disrupts AV node development. We sought to determine whether Notch signaling plays a role in the formation and function of the mammalian conduction system. To achieve this, we selectively inhibited Notch signaling within a subset of murine cardiomyocytes through Cre-inducible expression of a dominant-negative truncated form of mastermind-like protein (DNMAML). All 4 mammalian Notch receptors interact with mastermind-like proteins after ligand-mediated activation and translocation to the nucleus. DNMAML is a well-characterized truncated form of mastermind-like protein that acts as a specific and effective Notch inhibitor by binding to the Notch intracellular domain and preventing recruitment of coactivators (30). We used mice in which DNMAML (knocked into the constitutively active Rosa26 locus) is expressed in a tissue-specific manner after activation by Cre recombinase (31), and we crossed these mice with myosin light chain 2v$^{Cre/+}$ animals (*Mlc2v*$^{Cre/+}$ animals), which express Cre in embryonic ventricular myocytes and AV nodal cells (32, 33).

Mlc2v$^{Cre/+}$*DNMAML* mice are viable, with normal appearing cardiac structures and normal function as assessed by echocardiography (Supplemental Table 1; supplemental material available online with this article; doi:10.1172/JCI44470DS1). However, *Mlc2v*$^{Cre/+}$*DNMAML* mice had a significantly smaller AV node volume indexed to heart weight when compared with that of controls ($16 \pm 5.1 \times 10^6$ vs. $30 \pm 1.8 \times 10^6$ μm^3/g; n = three 5-month-old mice of each genotype; $P < 0.01$), as demonstrated by 3D reconstruction of the AV node from a representative control and Notch-inactivated mutant (Figure 1, A–D, and Supplemental Figure 1). Consistent with this observation, *Mlc2v*$^{Cre/+}$*DNMAML* mice had fewer cells expressing the hyperpolarization-activated cyclic nucleotide-gated channel 4 (HCN4), which contributes to the hyperpolarization current of AV nodal tissue and is a marker of cells within the proximal AV node (Figure 1, E and F). Collagen I staining demonstrated a grossly intact annulus fibrosis (Figure 1, G and H).

Cx30.2 is a low conductance gap junction isoform expressed in the murine compact AV node and inferior nodal extension that decelerates electrical impulse propagation, while Cx40 expression within the AV node is confined to the lower AV nodal cells that are contiguous with the His bundle and contribute to faster electrical conduction (3, 34). Myocytes of the compact AV node and inferior nodal extension are derived from AV canal myocardium, while Cx40-positive lower AV nodal cells and the His bundle are derived from ventricular myocardium (3, 34). *Mlc2v*$^{Cre/+}$*DNMAML* mice demon-

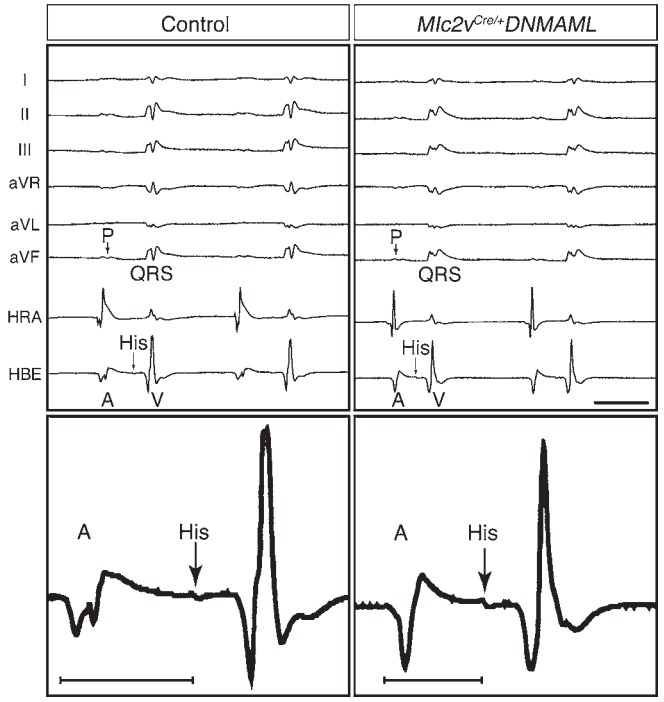

Figure 2
Notch inhibition disrupts AV nodal delay. The top panels show representative 6-lead EKG and intracardiac electrograms from the high right atrium (HRA) and His bundle electrogram (HBE), demonstrating shorter PR and AH intervals in *Mlc2v*$^{Cre/+}$*DNMAML* mice when compared with those in control mice. A, atrial depolarization; P, P wave; V, ventricular depolarization. Scale bar: 50 ms. The bottom panels show 1 representative beat from the His bundle electrogram at higher magnification, with the AH interval demarcated by the bars. The control AH interval was 33 ms, and the *Mlc2v*$^{Cre/+}$*DNMAML* AH interval was 22 ms. Control mice are *DNMAML* littermates of *Mlc2v*$^{Cre/+}$*DNMAML* mice.

strated a selective loss of Cx30.2-expressing cells within the compact AV node and inferior nodal extension, with a maintenance of Cx40-expressing lower nodal cells (Figure 1, I and J), suggesting a specific loss of AV canal–derived tissue in Notch loss-of-function mutants.

Notch inhibition disrupts AV nodal delay. It has previously been shown that Cx30.2 null mice have accelerated AV conduction, with a concomitantly shortened PR interval compared with that of wild-type mice (35). Global knockout of both Cx30.2 and Cx40 results in restoration of normal AV delay, suggesting that the ratio of connexin isoforms within the AV nodal interface is important for fine-tuning AV delay (36). Given the altered connexin isoform ratio seen in *Mlc2v*$^{Cre/+}$*DNMAML* mice, AV conduction was assessed via surface electrocardiogram (EKG) in anesthetized animals using either pentobarbital (Figure 2 and Table 1) or isoflurane (Supplemental Results). This analysis revealed a reproducibly shorter PR interval in Notch-inhibited hearts when compared with that of littermate control hearts (43.0 ± 4.2 vs. 37.5 ± 2.5 ms; $n = 7$ control and $n = 6$ *Mlc2v*$^{Cre/+}$*DNMAML* mice at 5 months; $P < 0.02$), while the QRS interval and QT interval corrected for murine physiology (QT_m) were unchanged (Table 1). Tissue-specific deletion of the Notch1 receptor in myocardium (*Mlc2v*$^{Cre/+}$*Notch1*$^{flox/flox}$) also resulted in shortening of the PR interval (Supplemental Table 2), suggesting that inhibition of Notch1 receptor activity is at least in part responsible for the observed phenotype in DNMAML mice.

Invasive electrophysiology studies demonstrated a shorter atriohisian (AH) interval in Notch-inactivated hearts when compared with that of control hearts (35.6 ± 4.5 vs. 28.1 ± 4.5 ms; $n = 9$ control hearts and $n = 8$ *Mlc2v*$^{Cre/+}$*DNMAML* hearts; $P < 0.004$), consistent with accelerated AV conduction, while the remainder of the ventricular conduction system parameters appear unaffected (Table 1). During programmed electrical stimulation, the reduction in the AH interval of mutants occurred at every conduction interval tested (Supplemental Figure 2). Another defining characteristic of AV nodal tissue is a relatively long refractory period, or recovery time after being excited, which has evolved to protect the ventricles from rapidly conducting atrial tachyarrhythmias. Notch-inactivated hearts demonstrate a shorter AV effective refractory period (AVERP) when compared with that of control hearts (66.1 ± 4.9 vs. 57.5 ± 7.6 ms, $n = 9$ control hearts and $n = 8$ *Mlc2v*$^{Cre/+}$*DNMAML* hearts; $P < 0.02$), confirming defective AV nodal function.

Notch activation produces accessory pathways. To gain further insight into the role of Notch in the morphogenesis of the AV canal, we used mice in which the *Notch1* intracellular domain (NICD, knocked into the constitutively active Rosa26 locus) is expressed in a tissue-specific manner after activation by Cre recombinase (37), and we crossed these mice with *Mlc2v*$^{Cre/+}$ mice. NICD functions in a ligand-independent fashion to translocate to the nucleus and recruit coactivators to induce transcription of Notch target genes.

Mlc2v$^{Cre/+}$*NICD* mice were viable, with no gross structural abnormalities evident at birth. However, by the first week of life excess tissue was noted along the right AV junction, which was confirmed by scanning electron microscopy (Figure 3, A and B). Histologic characterization of

Table 1
Notch inhibition disrupts AV nodal delay

Electrocardiography

	Control ($n = 7$)	*Mlc2v*$^{Cre/+}$*DNMAML* ($n = 6$)
HR (bpm)	406 ± 62	488 ± 47[A]
PR (ms)	43.0 ± 4.2	37.5 ± 2.5[A]
QRS (ms)	9.3 ± 2.4	8.0 ± 0.6
QT_m (ms)	32.9 ± 3.8	35.0 ± 3.2

Electrophysiology

	Control ($n = 9$)	*Mlc2v*$^{Cre/+}$*DNMAML* ($n = 8$)
HR (bpm)	424 ± 63	479 ± 42[A]
AH (ms)	35.6 ± 4.5	28.1 ± 4.5[B]
Hd (ms)	4.4 ± 0.8	4.1 ± 0.6
HV (ms)	12.1 ± 1.7	12.0 ± 1.6
$SNRT_{120}$ (ms)	172 ± 27	166 ± 43
$AVERP_{120}$ (ms)	66.1 ± 4.9	57.5 ± 7.6[A]
$AERP_{120}$ (ms)	39.4 ± 8.5	35.8 ± 7.0
AVWBCL	89.4 ± 8.5	82.5 ± 6.5
AV 2:1	72.8 ± 9.4	65.0 ± 7.1
$VERP_{120}$ (ms)	40.6 ± 9.8	28.8 ± 7.0

Mean ± SD. [A]$P < 0.05$ for control littermate *DNMAML* versus *Mlc2v*$^{Cre/+}$*DNMAML* mice; [B]$P < 0.01$ for control *DNMAML* versus *Mlc2v*$^{Cre/+}$*DNMAML* mice. HR, heart rate; AH, AH interval; Hd, His duration; HV, His-ventricular interval; $SNRT_{120}$, sinus node recovery time at drive train of 120 ms; $AVERP_{120}$, AVERP at 120 ms; $AERP_{120}$, atrial effective refractory period at 120 ms; AVWBCL, AV Wenckebach block cycle length; AV 2:1, AV 2:1 block cycle length; $VERP_{120}$, ventriculoatrial effective refractory period at 120 ms.

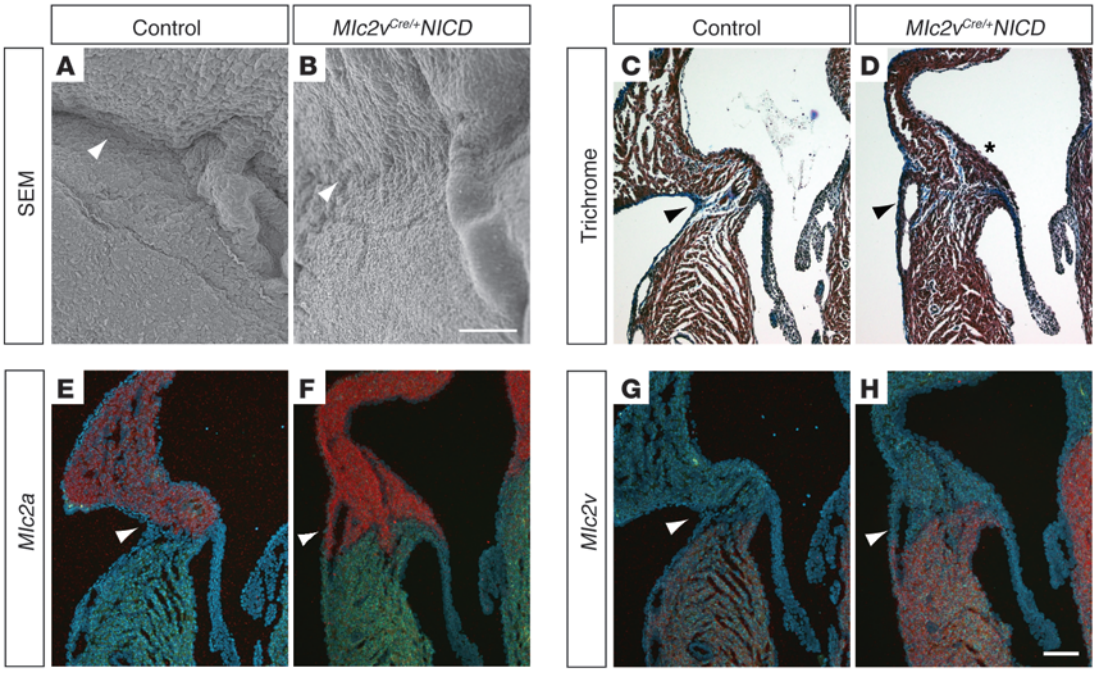

Figure 3
Activation of Notch signaling results in accessory pathway formation. (**A** and **B**) Scanning electron microscopy demonstrates excess tissue in the right AV junction of 1-week-old *Mlc2v*$^{Cre/+}$*NICD* mice (arrow in **B**) when compared with that of control mice, which have a distinct AV groove (arrow in **A**). Scale bar: 100 μm (**A** and **B**). (**C** and **D**) Masson's trichrome staining of postnatal day 3 hearts reveals an epicardial accessory pathway traversing the AV groove in Notch-activated hearts (arrow, **D**), connecting atrial and ventricular myocardium, while the AV groove from a similar region in control hearts contains no myocardial tissue (arrow, **C**). Note the presence of myocardial tissue along the atrial side of the tricuspid valve (asterisk, **D**). (**E**–**H**) In situ hybridization reveals that accessory pathways express (**F**) the atrial marker *Mlc2a* (red) near the atrium and (**H**) *Mlc2v* (red) near the ventricle. Arrowheads in **E** and **G** denote the AV groove, and arrowheads in **F** and **H** denote an epicardial accessory pathway. Scale bar: 100 μm (**C**–**H**). Control mice are *NICD* littermates of *Mlc2v*$^{Cre/+}$*NICD* mice.

the AV junction in Notch-activated hearts revealed muscular connections between the atrial and ventricular myocardium extrinsic to the AV node. Ectopic myocardium spanning the AV junction was most commonly epicardial and occurred on the right side (Figure 3D and Supplemental Figure 3C), but left-sided connections and those crossing the annulus fibrosus septally were also often noted (n = 8 postnatal mice). Muscular connections along the right AV junction expressed the atrial marker myosin light chain 2a (*Mlc2a*) in the myocardium closest to the atrium and the ventricular marker *Mlc2v* near the ventricle (Figure 3, E–H). Although marker expression does not provide direct evidence for the developmental origin of the tissue, these findings are consistent with a hypothesis that functional accessory pathways derive from AV canal myocardium capable of differentiating into either atrial or ventricular tissue. Furthermore, an expanded region of AV canal–derived AV nodal tissue (Cx30.2 positive, Tbx3 positive, and Cx40 negative) could be found within the base of the interatrial septum (Supplemental Figure 4). We also noted the unusual and striking persistence of myocardium along the atrial surface of the AV valves (Figure 3D and Supplemental Figure 3C). Myocytes derived from AV canal myocardium populate the AV valves during embryogenesis, but this tissue normally regresses by late gestation (38).

We examined histology and gene expression of staged embryos from E10.5–E18.5 to determine the earliest signs of detectable defects in *Mlc2v*$^{Cre/+}$*NICD* specimens. *Bmp2* was expressed by AV canal myocardium of control embryos at E10.5 and E12.5 (Figure 4, A and B), and expression was unchanged in mutants at these stages (Figure 4, F and G). Subsequent to E12.5, *Bmp2* expression diminished significantly in this region. Hence, we examined *Tbx3* expression at E15.5 and E17.5 to identify AV canal myocardium at these time points. In control embryos (Figure 4, C and D), a sharp boundary of expression was present between the thin rim of remaining AV canal myocardium and ventricular tissue. However, in mutant embryos (Figure 4, H and I), *Tbx3* expression was slightly expanded and the boundary was irregular, especially at E17.5 in the region of the right posterior AV junction. At E16.5, coronary veins of control embryos could be identified in the AV groove (asterisks, Figure 4E). In mutant embryos, the coronary veins were enlarged and were surrounded by a muscular wall expressing myosin, as detected by MF-20 antibody staining (Figure 4J). Muscularization and structural abnormalities of coronary veins have been identified in humans with WPW, in which this tissue may contribute to accessory pathways (Supplemental Figure 3B and refs. 39–41). Hence, developmental abnormalities were first noted at approximately E15.5 in *Mlc2v*$^{Cre/+}$*NICD* embryos and were consistent with an excess of AV canal–derived tissue.

Notch activation produces ventricular preexcitation and atrial arrhythmias in a mouse model of WPW. To determine the functional consequences of the structural abnormalities in Notch-activated mice, serial surface ECGs were performed. At birth, Notch-activated mice had normal electrical activation (n = 7, Supplemental Figure 5A). However, by postnatal day 2, 1 out of 7 mice examined developed electrocardiographic changes suggestive of ventricular preexcitation, as evidenced by a short PR interval, wide QRS, and delta wave (data not shown). By

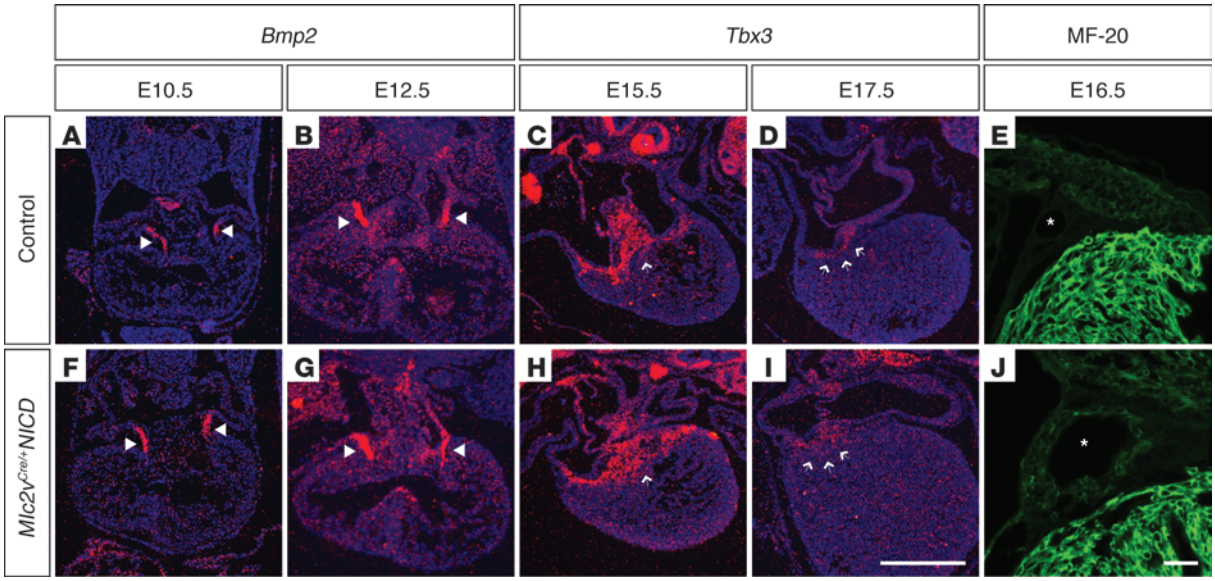

Figure 4
Developmental analysis reveals late gestation AV canal defects in *Mlc2v*$^{Cre/+}$*NICD* embryos. In situ hybridization of staged embryos from E10.5–E18.5 was performed to determine the earliest signs of detectable AV canal defects in *Mlc2v*$^{Cre/+}$*NICD* specimens. (**A** and **B**) *Bmp2* is expressed in AV canal myocardium of control embryos at E10.5 and E12.5, and (**F** and **G**) expression is unchanged in mutants. (**C** and **D**) *Tbx3* marks AV canal myocardium in the posterior region of the heart at E15.5 and E17.5 and reveals a sharp boundary of expression between the thin rim of remaining AV canal myocardium and ventricular tissue in controls. (**H** and **I**) In mutant embryos, *Tbx3* expression is slightly expanded and the boundary is irregular, especially at E17.5 (arrows, **I**). (**E** and **J**) MF-20 antibody staining for myosin expression at E16.5 identifies coronary veins of control embryos in the AV groove (asterisk in **E**). In mutant embryos, the coronary veins were enlarged and were surrounded by a muscular wall expressing myosin (asterisk in **J**). Arrowheads denote the AV canal in **A**, **B**, **F**, and **G**, and arrows denote the boundary between AV canal tissue and ventricular tissue in **C**, **D**, **H**, and **I**. Scale bar: 500 μm (**A**–**D** and **F**–**I**); 50 μm (**E** and **J**). Control embryos are *NICD* littermates of *Mlc2v*$^{Cre/+}$*NICD* embryos.

1 week of age, 6 out of 7 mice developed these electrocardiographic changes (Supplemental Figure 5B), and by 8 weeks, 100% of a much larger cohort of Notch-activated mice had electrocardiographic changes suggestive of ventricular preexcitation ($n > 50$). Invasive electrophysiology studies of adult Notch-activated hearts confirmed robust ventricular preexcitation and findings consistent with the presence of rapidly conducting accessory pathways (Figure 5). Abnormally rapid AV conduction was present at baseline and with programmed stimulation in all mutant animals examined ($n = 7$), which was significantly faster than that of littermate controls (Table 2). Even at the shortest cycle length at which our system could pace the atrium of Notch-activated hearts (50 ms or 1,200 bpm), AV conduction remained fixed at a 1:1 ratio, whereas control hearts would exhibit AV conduction block at paced atrial rates greater than approximately 600 bpm (Table 2). Consistent with these findings, the AVERP in Notch-activated hearts was significantly shorter than that in littermate controls (Table 2).

As previously mentioned, WPW patients have a high prevalence of atrial fibrillation, which can lead to rapid activation of the ventricles via the accessory pathway. Notch-activated hearts were also greatly predisposed to the development of atrial tachycardias during programmed electrical stimulation (Table 2), often occurring with the introduction of just a single atrial extrastimulus and resulting in a rapid ventricular response.

Further confirmation of ventricular preexcitation is provided by high-resolution optical mapping studies that delineate the spatial and temporal pattern of depolarization throughout the cardiac cycle. In control hearts, optical mapping studies demonstrated that electrical activation began with atrial depolarization, followed by an AV delay, and then ventricular depolarization. Ventricular depolarization began at the apex of the right and left ventricles and ended near the AV groove (Figure 6, A, B, and E, and Supplemental Video 1). In striking contrast, adult Notch-activated hearts revealed atrial depolarization, followed by immediate ventricular depolarization that traveled from base to apex, without an AV delay (Figure 6, C, D, and F, and Supplemental Video 2). Right-sided posterior breakthrough was noted in all 8 mutant animals that were examined, and 5 of these also showed evidence of additional left- and right-sided breakthroughs, indicating the presence of multiple accessory pathways. The high incidence of right-sided preexcitation was consistent with the preponderance of accessory pathway tissue identified by histology in this location. Echocardiography of adult *Mlc2v*$^{Cre/+}$*NICD* animals revealed normal fractional shortening and ejection fraction when compared with those of control littermates (Supplemental Table 3), but the contraction pattern of the heart was markedly abnormal, consistent with the activation patterns obtained by optical mapping (Supplemental Videos 3 and 4).

Discussion

In this report, we provide evidence from both gain-of-function and loss-of-function approaches to support a model in which Notch activity is required for proper maturation of AV canal myocardium, which normally contributes to the AV node and therefore significantly impacts cardiac conduction (3, 42). Inhibition of Notch signaling affects the structure and function of the mature AV node by reducing overall size and by producing a specific loss of slowly conducting Cx30.2-expressing cells derived from AV canal myocar-

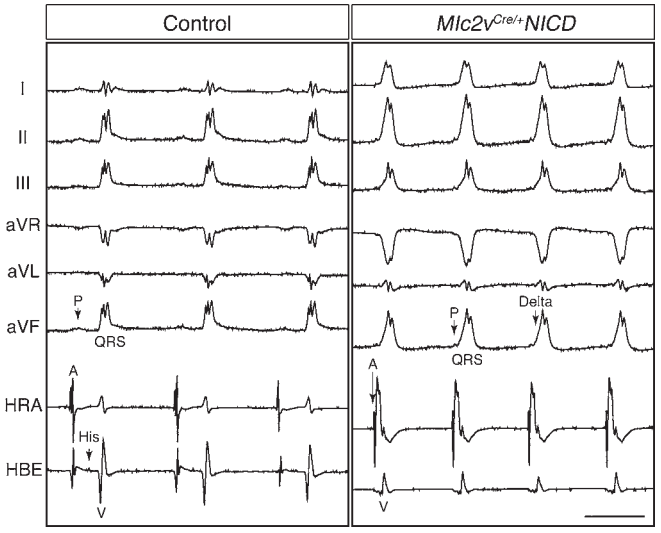

Figure 5
Notch activation leads to ventricular preexcitation. Representative 6-lead EKG tracings and intracardiac electrograms from the high right atrium and His bundle electrogram are shown from a control and *Mlc2v*$^{Cre/+}$*NICD* mouse. Note the fused p wave (P) and QRS complexes and widened QRS with delta wave on surface EKG as well as the fused atrial (A) and ventricular (V) electrograms in Notch-activated mice, indicative of robust AV conduction over the accessory pathway. Scale bar: 100 ms. Control mice are *NICD* littermates of *Mlc2v*$^{Cre/+}$*NICD* mice.

dium, while rapidly conducting Cx40-expressing cells derived from ventricular myocardium (34) are preserved. Tissue-specific deletion of the Notch1 receptor in myocardium also resulted in shortening of the PR interval (Supplemental Table 2), suggesting that inhibition of Notch1 receptor activity is at least in part responsible for the observed phenotype in *Mlc2v*$^{Cre/+}$*DNMAML* mice.

The cardiac phenotype produced by our Notch gain-of-function model is strikingly reminiscent of human ventricular preexcitation syndromes, such as WPW. Many of the early reports of this disorder described epicardial bands of ectopic myocardium spanning the AV groove (Supplemental Figure 3A), and early treatments included surgical disruption of these epicardial accessory pathways (43). Ectopic tissue spanning the AV boundary in our mouse model was evident by gross inspection and by scanning electron microscopy (Figure 3B). A wide range of additional locations of accessory pathways have been described in humans, including those traversing the annulus fibrosus, epicardial and subendocardial tracts on both right and left sides, and myocardial cuffing of the coronary veins. We identified related examples in our mouse model. To our knowledge, this is the first animal model of preexcitation with a predisposition to atrial arrhythmias, an important cause of morbidity and mortality in patients. Interestingly, although subtle histologic and gene expression defects could be identified as early as E15.5, mice did not display electrocardiographic evidence of ventricular preexcitation until several days or more after birth. We attribute this to physiologic mechanisms that contribute to AV delay prior to maturation of the annulus fibrosis as well as the substantial expansion of ectopic myocardial tissue within the region of the AV junction noted to occur after birth (data not shown).

Previously, transgenic mice were generated to model a relatively rare form of WPW, in which the *PRKAG2* gene is mutated (44, 45). These animals also develop ventricular preexcitation in the postnatal period (46), and electrophysiologic defects are associated with abnormally increased glycogen storage in myocardium and cardiac hypertrophy (21). Breeches in the annulus fibrosus allow for electrical communication between atria and ventricles. While these studies allow for further investigation of the underlying mechanisms of ventricular preexcitation in some contexts, transgenic *PRKAG2* mice are probably not optimal models for the more common forms of isolated ventricular preexcitation seen clinically. Further, it is likely that the underlying mechanisms of bypass tract formation are distinct in the Notch and PRKAG2 models, because we observe epicardial accessory pathways and ectopic myocardium, including muscularized coronary veins, which cannot be explained by a breakdown or breech of the annulus fibrosus.

The annulus fibrosus derives from epicardial cells, and recent studies in developing chick embryos demonstrate that mechanical interruption of epicardial cell migration can disrupt annulus fibrosus formation, with resulting ventricular preexcitation (10). Therefore, we propose that ventricular preexcitation can result from at least 2 distinct mechanisms (which are not mutually exclusive). First, defects in formation or maintenance of the annulus fibrosus may allow for electrical continuity between atrial and ventricular tissue. Second, abnormal patterning of AV canal myocardium may result in ectopic myocardial tissue and accessory pathways that can bypass a well-formed annulus. We propose that genetic, epigenetic, or environmental mechanisms that activate components of the Notch signaling cascade may cause patterning defects of AV canal myocardium and WPW. While this possibility, among others, has been previously suggested as a potential cause of WPW, we believe that our data and robust animal model that mimics the human disease provide strong experimental support for this hypothesis. However, as Notch signaling is known to be involved in cell-cell signaling, it is possible that activation or inhibition of Notch in AV canal myocardium can lead to indirect effects on neighboring epicardial or endocardial cells, which may contribute to the observed phenotypes. For example, it was recently demonstrated that constitutive Notch1 activation at early developmental stages in murine AV canal myocardium results in abnormal endocardial epithelial-to-mesenchymal transition (47). Additional support in the future may derive from genetic fate-map-

Table 2
Notch activation leads to ventricular preexcitation

	Control (n = 6)	*Mlc2v*$^{Cre/+}$*NICD* (n = 7)
HR (bpm)	393 ± 86	464 ± 54
AVI (ms)	45 ± 5	11 ± 1[A]
$SNRT_{120}$ (ms)	186 ± 45	163 ± 39
$AVERP_{120}$ (ms)	62 ± 11	≤34[B]
$AERP_{120}$ (ms)	33 ± 7	34 ± 7
AV pace 1:1	95 ± 11	≤50[A]
VA pace 1:1	108 ± 21	≤50[A]
$VERP_{120}$ (ms)	31 ± 11	39 ± 8
Episodes AT	0	24
Duration AT (s)	–	2.3
AT CL (ms)	–	44
Mice with AT	0/6	7/8[C]

Mean ± SD. [A]$P < 4 \times 10^{-5}$ for control versus *Mlc2v*$^{Cre/+}$*NICD* mice; [B]$P < 0.0003$ for control versus *Mlc2v*$^{Cre/+}$*NICD* mice; [C]$P < 0.01$ for control versus *Mlc2v*$^{Cre/+}$*NICD* mice. Controls are littermate *NICD* mice. AVI, AV interval; AV pace 1:1, AV 1:1 conduction cycle length (CL); VA pace 1:1, ventriculoatrial 1:1 conduction cycle length; AT, atrial tachycardia.

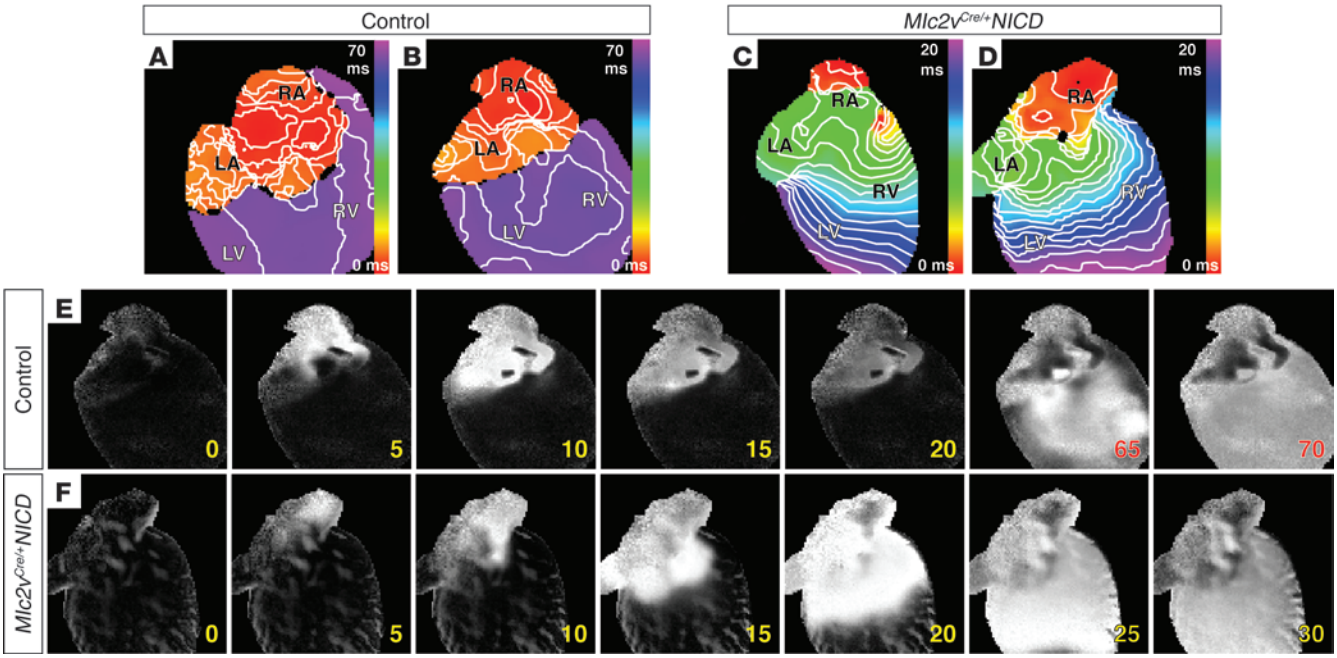

Figure 6

Activation of Notch signaling leads to ventricular preexcitation. Electrical activation maps from the posterior surface of the heart, with 1-ms contour lines for (**A** and **B**) control and (**C** and **D**) *Mlc2v*$^{Cre/+}$*NICD* hearts. Note the different time scales. Atrial activation in control hearts is followed by a significant AV delay prior to ventricular activation. In Notch-activated hearts, the electrical impulse travels from the atria into the ventricles without AV delay via (**C**) an accessory pathway along the right posterior surface or via (**D**) dual accessory pathways in the right and left posterior regions, resulting in abnormal activation of the ventricles from base to apex. (**E** and **F**) Still frame activation images of the hearts from **B** and **D**, taken every 5 ms, in which a time gap of 45 ms, corresponding to AV delay, is denoted in **E** by a change from yellow to red numbers. White tissue is depolarized. RA, right atrium; LA, left atrium. Control mice are *NICD* littermates of *Mlc2v*$^{Cre/+}$*NICD* mice.

ping studies to rigorously determine adult derivatives of AV canal myocardium in Notch-activated hearts. However, technical limitations preclude this approach at the present time, since Cre-reporter mice cannot be used to track AV canal myocardial derivatives, because our model uses Cre in alternative tissues to activate Notch.

Notch plays reiterated and complex roles during many stages of cardiovascular development (48), and prior work has suggested that Notch participates in early boundary formation of the AV canal. For example, in chick embryos, activated Notch2 or overexpression of Hesr1 (also known as Hey1) or Hesr2 (also known as Hey2) (downstream mediators of Notch signaling) can function to repress *Bmp2*, and this has been proposed as a mechanism by which Notch activity in atria and ventricles can help to restrict *Bmp2* expression to the AV canal (6). In the mouse, *Hesr1* and *Hesr2* are expressed in the forming atria and ventricles, respectively, and misexpression of either gene throughout the heart represses AV myocardium formation and downregulates *Tbx2* and *Bmp2* (5). Overexpression of NICD using the *Mesp1*$^{Cre/+}$ driver to activate expression very early during heart formation results in suppression of AV canal myocardium and related marker genes (12). These studies, and others, provide data to support a model in which Notch activity in working atrial and ventricular myocardium suppresses *Bmp2* and AV canal myocardial fate, while Bmp2 normally activates *Tbx2/3* expression, which instructs AV myocardial maturation (42, 49). Our findings are generally consistent with this model, although patterning defects in our animal models did not occur until later in development than seen in the prior studies. It is likely that Notch plays reiterative roles during maturation of the heart and, specifically, of AV canal myocardium, and specific downstream pathways may vary with developmental stage and context. For example, we did not observe a decrease in *Bmp2* or *Tbx3* expression in our Notch-activated hearts, as might have been predicted from studies performed at earlier developmental stages (5, 6, 12).

Our analysis of *Mlc2v*$^{Cre/+}$*NICD* animals focused on structural defects likely to be involved in ventricular preexcitation. However, we also uniformly observed the presence of ectopic myocardium along the atrial surface of the AV valve leaflets that we also attributed to persistence of AV canal myocardium. It is interesting to note that a similar pattern of ectopic myocardium has been frequently reported in patients with Ebstein's anomaly (50), which is strongly associated with WPW. Although we did not observe other features of Ebstein's anomaly in our mouse model, such as atrialization of the right ventricle, it will be of interest to determine whether developmental defects of AV canal myocardium are responsible for some features of this rare disorder.

In summary, genetic manipulation of Notch activity provides experimental evidence to support a developmental model to explain common forms of WPW and ventricular preexcitation syndrome. AV canal myocardium, which functions in the embryo to delay AV conduction, undergoes late gestation remodeling, regresses, and gives rise to the AV node. We propose that abnormal patterning of AV canal–derived myocardium, under the influence of active Notch signaling, can result in functional accessory pathways and arrhythmias. Further delineation of the molecular cascades responsible for normal remodeling and maturation of AV canal myocardium will inform the genetic and developmental understanding of WPW and related disorders.

Methods

Mice. *Mlc2v*$^{Cre/+}$, *DNMAML*, and *NICD* mice were maintained on a mixed background and were genotyped using Cre-specific primers (5′-ATTCTCCCACCGTCAGTACG-3′ and 5′-CGTTTTCTGAGCATACCTGGA-3′) and primers specific for the ROSA26 locus (5′-AAAGTCGCTCTGAGTTGTTAT-3′, 5′-GCGAAGAGTTTGTCCTCAACC-3′, and 5′-GGAGCGGGAGAAATGGATATG-3′). Littermate animals were compared in all experiments unless otherwise noted. All animal protocols were approved by the University of Pennsylvania Institutional Animal Care and Use Committee.

Histology, immunohistochemistry, and in situ hybridization. AV node volume was measured in 3 control *Mlc2v*$^{+/+}$*DNMAML* and 3 *Mlc2v*$^{Cre/+}$*DNMAML* adult hearts using Masson's trichrome staining of sections through the entire AV node, including the compact AV node, inferior nodal extension, and lower nodal cells (34). The presence of connective tissue located between AV nodal tissue and the surrounding atrial and AV ring myocardium as well as the distinct morphology of the AV nodal cells allowed identification of the AV node. Quantification of AV nodal area was performed on every third section using ImageJ software (http://rsbweb.nih.gov/ij/), and AV node volume was subsequently calculated. 3D reconstruction was performed by importing the images into Amira 5.3.1 (Visage Imaging GmbH). Sections were aligned, and the labeling function was used to identify and draw discrete cardiac subcompartments, including atrial tissues, tricuspid valve, ventricular myocardium, and AV node, using a drawing tablet. The resulting labeled fields were then rendered into 3D surfaces with minimal smoothing to prevent data loss.

Immunohistochemistry was performed on frozen sections with antibodies recognizing HCN4 (H-300, Santa Cruz Biotechnology Inc.), Cx40 (C-20, Santa Cruz Biotechnology Inc.), Cx43 (C8093, Sigma-Aldrich), Cx30.2 (gift from Klaus Willecke, University of Bonn, Bonn, Germany), and Collagen I (MD Bioscience). Secondary antibody fluorescent conjugates included anti-rabbit Alexa 488 (Invitrogen), anti-goat Alexa 633 (Invitrogen), and anti-mouse TRITCRedx100 (Jackson ImmunoResearch Laboratories Inc.). Images were captured by sequentially scanning 3 channels using a Leica SP5 laser scanning confocal microscope. MF-20 antibody staining was performed on paraffin-embedded sections with antibody from the Hybridoma Bank. Radioactive in situ hybridizations were performed on samples that were fixed overnight with 4% paraformaldehyde, dehydrated through an ethanol series, paraffin embedded, and sectioned using previously described probes for *Mlc2a* and *Mlc2v* (51), *Bmp2* (52), and *Tbx3* (53). Histology, immunohistochemistry, and in situ hybridization images were analyzed using Adobe Photoshop. Control and mutant images were treated identically in all cases in which brightness and contrast were altered.

Echocardiography. Mice were anesthetized using an integrated isoflurane-based system. Two-dimensional images were obtained at 180 frames per second, using a 30-MHz probe (RMV 707B, Visual Sonics) in the parasternal long- and short-axis views to guide M-mode analysis at the midventricular level. Left ventricular fractional shortening, ejection fraction, and wall dimensions were computed from M-mode measurements.

EKG analysis. EKGs were performed on mice anesthetized with inhaled isoflurane for less than 5 minutes (Supplemental Figure 5 and Supplemental Table 2), except during invasive electrophysiology experiments (see below). Lead II EKGs were recorded at a sampling rate of 4,000 Hz (ADInstruments). EKG intervals were measured by averaging 100 beats using the LabChart software package (ADInstruments); measurements were taken by an investigator who was blinded to the genotypes of the mice.

Electrophysiology. Protocols for the in vivo mouse electrophysiology have been described in detail (46, 54). Mice were anesthetized with pentobarbital (33 mg/kg i.p.) and laid down on a heating pad to maintain core body temperature, and limb leads were placed subcutaneously to obtain multilead ECGs. An octapolar 1.7-French electrode catheter (CIBer mouse-EP, NuMED) was placed in the right atrium and ventricle under electrogram guidance through a jugular vein cutdown. A programmed digital stimulator (DTU-215, Fisher Scientific) delivered electrical impulses at approximately twice diastolic threshold, while surface ECG and intracardiac electrograms were displayed on a multichannel oscilloscope recorder (Bard Electrophysiology Inc.) and analyzed offline. Standard pacing protocols were used to assess atrial and ventricular conduction and refractoriness. Measurement of intervals was performed by 2 independent investigators who were blinded to the genotype of the mice.

Scanning electron microscopy. These experiments were carried out at CDB/CVI Microscopy Core (School of Medicine, University of Pennsylvania). Samples were fixed overnight in 4% paraformaldehyde and dehydrated in a graded ethanol series, followed by immersion twice for 10 minutes in 100% HMDS (Sigma-Aldrich), followed by 30 minutes of air drying, as described previously (55). Then samples were mounted on stubs and sputter coated with gold palladium. Specimens were observed and photographed using a Philips XL20 scanning electron microscope (FEI) at 10 kV accelerating voltage.

Optical mapping. Perfused hearts were optically mapped as described previously (56, 57). In brief, mice were heparinized (10,000 IU i.p.) and euthanized with 100% CO_2, followed by cervical dislocation. Hearts were extracted through a median sternotomy, and the aorta was cannulated and Langendorff perfused with a constant pressure of 68–74 mmHg (1.5–2.0 ml/min) with 38°C oxygenated (95% O_2 5% CO_2) modified Tyrode's solution containing 1.8 mM $CaCl_2$, 1.0 mM $MgCl_2$, 1.2 mM KH_2PO_4, 130 mM NaCl, 4.7 mM KCl, 24 mM $NaHCO_3$, 11.1 mM glucose, 0.052 g/l albumin, pH 7.4. Blebbistatin (5 mM) was used to limit motion artifacts (58). After 10 minutes of perfusion and equilibrium, hearts were injected with 20 mM voltage-sensitive fluorescent dye di-4-ANNEPS (Invitrogen), and uniform fluorescent saturation was reached in 10 minutes. High-resolution optical mapping studies were performed on an upright microscope (BX51WI, Olympus Inc.) outfitted with a high-speed CMOS camera (MiCAM ULTIMA L, SciMedia Ltd.).

Statistics. Student's 2-tailed *t* test analysis was used to evaluate differences between groups in all cases, except when comparing the number of mice with atrial tachycardia, for which a χ^2 analysis was used. Data are represented as mean ± SD. *P* values of less than 0.05 were considered statistically significant.

Acknowledgments

We would like to thank the members of the Epstein laboratory (especially Arun Padmanabhan) for many helpful discussions and technical support. We also thank Klaus Willecke for connexin-30.2 antibody. This work was supported by the University of Pennsylvania, Division of Cardiology T-32, and the Department of Medicine Measey Foundation Award to S. Rentschler, NIH National Center for Research Resources grant 5P20RR016434-09 to B.S. Harris, American Heart Association (AHA) Physician-Scientist/Post-Doctoral fellowship AHA 0825548D to R. Jain, NIH grant HL076751 to G.E. Morley, University of Pennsylvania Research Fund Award to V.V. Patel, and funds from the WW Smith Endowed Professorship, the NIH (U01HL100405, R01HL095634), and the AHA DeHaan Cardiac Myogenesis Center to J.A. Epstein.

Received for publication July 22, 2010, and accepted in revised form November 1, 2010.

Address correspondence to: Jonathan Epstein, 1154 BRB II, 421 Curie Blvd., Philadelphia, Pennsylvania 19087, USA. Phone: 215.898.8731; Fax: 215.573.2094; E-mail: epsteinj@mail.med.upenn.edu.

1. Bakker ML, Christoffels VM, Moorman AF. The cardiac pacemaker and conduction system develops from embryonic myocardium that retains its primitive phenotype. *J Cardiovasc Pharmacol*. 2010;56(1):6–15.
2. Christoffels VM, Smits GJ, Kispert A, Moorman AF. Development of the pacemaker tissues of the heart. *Circ Res*. 2010;106(2):240–254.
3. Aanhaanen WT, et al. The Tbx2+ primary myocardium of the atrioventricular canal forms the atrioventricular node and the base of the left ventricle. *Circ Res*. 2009;104(11):1267–1274.
4. Horsthuis T, et al. Gene expression profiling of the forming atrioventricular node using a novel tbx3-based node-specific transgenic reporter. *Circ Res*. 2009;105(1):61–69.
5. Kokubo H, Tomita-Miyagawa S, Hamada Y, Saga Y. Hesr1 and Hesr2 regulate atrioventricular boundary formation in the developing heart through the repression of Tbx2. *Development*. 2007;134(4):747–755.
6. Rutenberg JB, Fischer A, Jia H, Gessler M, Zhong TP, Mercola M. Developmental patterning of the cardiac atrioventricular canal by Notch and Hairy-related transcription factors. *Development*. 2006; 133(21):4381–4390.
7. Hahurij ND, et al. Accessory atrioventricular myocardial connections in the developing human heart: relevance for perinatal supraventricular tachycardias. *Circulation*. 2008;117(22):2850–2858.
8. Gittenberger-de Groot AC, Vrancken Peeters MP, Mentink MM, Gourdie RG, Poelmann RE. Epicardium-derived cells contribute a novel population to the myocardial wall and the atrioventricular cushions. *Circ Res*. 1998;82(10):1043–1052.
9. Zhou B, von Gise A, Ma Q, Hu YW, Pu WT. Genetic fate mapping demonstrates contribution of epicardium-derived cells to the annulus fibrosis of the mammalian heart. *Dev Biol*. 2010;338(2):251–261.
10. Kolditz DP, et al. Epicardium-derived cells in development of annulus fibrosis and persistence of accessory pathways. *Circulation*. 2008;117(12):1508–1517.
11. Milan DJ, Giokas AC, Serluca FC, Peterson RT, MacRae CA. Notch1b and neuregulin are required for specification of central cardiac conduction tissue. *Development*. 2006;133(6):1125–1132.
12. Watanabe Y, et al. Activation of Notch1 signaling in cardiogenic mesoderm induces abnormal heart morphogenesis in mouse. *Development*. 2006; 133(9):1625–1634.
13. Moskowitz IP, et al. The T-Box transcription factor Tbx5 is required for the patterning and maturation of the murine cardiac conduction system. *Development*. 2004;131(16):4107–4116.
14. Munshi NV, et al. Cx30.2 enhancer analysis identifies Gata4 as a novel regulator of atrioventricular delay. *Development*. 2009;136(15):2665–2674.
15. De Bacquer D, De Backer G, Kornitzer M. Prevalences of ECG findings in large population based samples of men and women. *Heart*. 2000;84(6):625–633.
16. Goudevenos JA, Katsouras CS, Graekas G, Argiri O, Giogiakas V, Sideris DA. Ventricular pre-excitation in the general population: a study on the mode of presentation and clinical course. *Heart*. 2000;83(1):29–34.
17. Munger TM, et al. A population study of the natural history of Wolff-Parkinson-White syndrome in Olmsted County, Minnesota, 1953–1989. *Circulation*. 1993;87(3):866–873.
18. Wan Q, Wu N, Fan W, Tang YY, Jin L, Fang Q. Clinical manifestations and prevalence of different types of supraventricular tachycardia among Chinese. *Chin Med J (Engl)*. 1992;105(4):284–288.
19. Doevendans PA, Wellens HJ. Wolff-Parkinson-white syndrome: a genetic disease? *Circulation*. 2001;104(25):3014–3016.
20. Follath F, Hallidie-Smith KA. Unusual electrocardiographic changes in Ebstein's anomaly. *Br Heart J*. 1972;34(5):513–519.
21. Arad M, et al. Constitutively active AMP kinase mutations cause glycogen storage disease mimicking hypertrophic cardiomyopathy. *J Clin Invest*. 2002;109(3):357–362.
22. Gollob MH, et al. Identification of a gene responsible for familial Wolff-Parkinson-White syndrome. *N Engl J Med*. 2001;344(24):1823–1831.
23. Blair E, et al. Mutations in the gamma(2) subunit of AMP-activated protein kinase cause familial hypertrophic cardiomyopathy: evidence for the central role of energy compromise in disease pathogenesis. *Hum Mol Genet*. 2001;10(11):1215–1220.
24. Le Gloan L, et al. A 8.26Mb deletion in 6q16 and a 4.95Mb deletion in 20p12 including JAG1 and BMP2 in a patient with Alagille syndrome and Wolff-Parkinson-White syndrome. *Eur J Med Genet*. 2008;51(6):651–657.
25. Lalani SR, et al. 20p12.3 microdeletion predisposes to Wolff-Parkinson-White syndrome with variable neurocognitive deficits. *J Med Genet*. 2009;46(3):168–175.
26. Stroud DM, et al. Abnormal conduction and morphology in the atrioventricular node of mice with atrioventricular canal targeted deletion of Alk3/Bmpr1a receptor. *Circulation*. 2007;116(22):2535–2543.
27. Gaussin V, et al. Alk3/Bmpr1a receptor is required for development of the atrioventricular canal into valves and annulus fibrosus. *Circ Res*. 2005; 97(3):219–226.
28. Li L, et al. Alagille syndrome is caused by mutations in human Jagged1, which encodes a ligand for Notch1. *Nat Genet*. 1997;16(3):243–251.
29. Oda T, et al. Mutations in the human Jagged1 gene are responsible for Alagille syndrome. *Nat Genet*. 1997;16(3):235–242.
30. Maillard I, et al. Mastermind critically regulates Notch-mediated lymphoid cell fate decisions. *Blood*. 2004;104(6):1696–1702.
31. High FA, et al. An essential role for Notch in neural crest during cardiovascular development and smooth muscle differentiation. *J Clin Invest*. 2007; 117(2):353–363.
32. Chen J, Kubalak SW, Chien KR. Ventricular muscle-restricted targeting of the RXRalpha gene reveals a non-cell-autonomous requirement in cardiac chamber morphogenesis. *Development*. 1998; 125(10):1943–1949.
33. Pashmforoush M, et al. Nkx2-5 pathways and congenital heart disease; loss of ventricular myocyte lineage specification leads to progressive cardiomyopathy and complete heart block. *Cell*. 2004;117(3):373–386.
34. Aanhaanen WT, et al. Developmental origin, growth, and three-dimensional architecture of the atrioventricular conduction axis of the mouse heart. *Circ Res*. 2010;107(6):728–736.
35. Kreuzberg MM, Willecke K, Bukauskas FF. Connexin-mediated cardiac impulse propagation: connexin 30.2 slows atrioventricular conduction in mouse heart. *Trends Cardiovasc Med*. 2006;16(8):266–272.
36. Schrickel JW, et al. Normal impulse propagation in the atrioventricular conduction system of Cx30.2/Cx40 double deficient mice. *J Mol Cell Cardiol*. 2009; 46(5):644–652.
37. Stanger BZ, Datar R, Murtaugh LC, Melton DA. Direct regulation of intestinal fate by Notch. *Proc Natl Acad Sci U S A*. 2005;102(35):12443–12448.
38. de Lange FJ, et al. Lineage and morphogenetic analysis of the cardiac valves. *Circ Res*. 2004;95(6):645–654.
39. Ho SY. Accessory atrioventricular pathways: getting to the origins. *Circulation*. 2008;117(12):1502–1504.
40. Schumacher B, Tebbenjohanns J, Pfeiffer D, Omran H, Jung W, Luderitz B. Prospective study of retrograde coronary venography in patients with posteroseptal and left-sided accessory atrioventricular pathways. *Am Heart J*. 1995;130(5):1031–1039.
41. Sun Y, et al. Coronary sinus-ventricular accessory connections producing posteroseptal and left posterior accessory pathways: incidence and electrophysiological identification. *Circulation*. 2002; 106(11):1362–1367.
42. Bakker ML, et al. Transcription factor Tbx3 is required for the specification of the atrioventricular conduction system. *Circ Res*. 2008;102(11):1340–1349.
43. Hanon S, Shapiro M, Schweitzer P. Early history of the pre-excitation syndrome. *Europace*. 2005;7(1):28–33.
44. Sidhu JS, et al. Transgenic mouse model of ventricular preexcitation and atrioventricular reentrant tachycardia induced by an AMP-activated protein kinase loss-of-function mutation responsible for Wolff-Parkinson-White syndrome. *Circulation*. 2005; 111(1):21–29.
45. Arad M, et al. Transgenic mice overexpressing mutant PRKAG2 define the cause of Wolff-Parkinson-White syndrome in glycogen storage cardiomyopathy. *Circulation*. 2003;107(22):2850–2856.
46. Patel VV, et al. Electrophysiologic characterization and postnatal development of ventricular pre-excitation in a mouse model of cardiac hypertrophy and Wolff-Parkinson-White syndrome. *J Am Coll Cardiol*. 2003;42(5):942–951.
47. Luna-Zurita L, et al. Integration of a Notch-dependent mesenchymal gene program and Bmp2-driven cell invasiveness regulates murine cardiac valve formation. *J Clin Invest*. 2010;120(10):3493–3507.
48. High FA, Epstein JA. The multifaceted role of Notch in cardiac development and disease. *Nat Rev Genet*. 2008;9(1):49–61.
49. Christoffels VM, Hoogaars WM, Tessari A, Clout DE, Moorman AF, Campione M. T-box transcription factor Tbx2 represses differentiation and formation of the cardiac chambers. *Dev Dyn*. 2004;229(4):763–770.
50. Anderson KR, Zuberbuhler JR, Anderson RH, Becker AE, Lie JT. Morphologic spectrum of Ebstein's anomaly of the heart: a review. *Mayo Clin Proc*. 1979;54(3):174–180.
51. Kuo CT, et al. GATA4 transcription factor is required for ventral morphogenesis and heart tube formation. *Genes Dev*. 1997;11(8):1048–1060.
52. Kaartinen V, Dudas M, Nagy A, Sridurongrit S, Lu MM, Epstein JA. Cardiac outflow tract defects in mice lacking ALK2 in neural crest cells. *Development*. 2004;131(14):3481–3490.
53. Chapman DL, et al. Expression of the T-box family genes, Tbx1-Tbx5, during early mouse development. *Dev Dyn*. 1996;206(4):379–390.
54. Ismat FA, et al. Homeobox protein Hop functions in the adult cardiac conduction system. *Circ Res*. 2005;96(8):898–903.
55. Braet F, De Zanger R, Wisse E. Drying cells for SEM, AFM and TEM by hexamethyldisilazane: a study on hepatic endothelial cells. *J Microsc*. 1997;186(pt 1):84–87.
56. Rentschler S, et al. Visualization and functional characterization of the developing murine cardiac conduction system. *Development*. 2001;128(10):1785–1792.
57. Morley GE, et al. Reduced intercellular coupling leads to paradoxical propagation across the Purkinje-ventricular junction and aberrant myocardial activation. *Proc Natl Acad Sci U S A*. 2005; 102(11):4126–4129.
58. Fedorov VV, et al. Application of blebbistatin as an excitation-contraction uncoupler for electrophysiologic study of rat and rabbit hearts. *Heart Rhythm*. 2007;4(5):619–626.